Journal of Sound and Vibration 349 (2015) 276–288

Contents lists available at ScienceDirect

Journal of Sound and Vibration

journal homepage: www.elsevier.com/locate/jsvi

Interpreting the forced responses of a two-degree-of-freedom nonlinear oscillator using backbone curves

T.L. Hill [a,*], A. Cammarano [b], S.A. Neild [a], D.J. Wagg [c]

[a] Department of Mechanical Engineering, University of Bristol, Bristol BS8 1TR, UK
[b] School of Engineering, University of Glasgow, Glasgow G12 8QQ, UK
[c] Department of Mechanical Engineering, University of Sheffield, Sheffield S1 3JD, UK

ARTICLE INFO

Article history:
Received 14 November 2014
Received in revised form
26 February 2015
Accepted 14 March 2015
Handling Editor: W. Lacarbonara
Available online 21 April 2015

ABSTRACT

In this paper the backbone curves of a two-degree-of-freedom nonlinear oscillator are used to interpret its behaviour when subjected to external forcing. The backbone curves describe the loci of dynamic responses of a system when unforced and undamped, and are represented in the frequency–amplitude projection. In this study we provide an analytical method for relating the backbone curves, found using the second-order normal form technique, to the forced responses. This is achieved using an energy-based analysis to predict the *resonant crossing points* between the forced responses and the backbone curves. This approach is applied to an example system subjected to two different forcing cases: one in which the forcing is applied directly to an underlying linear mode and the other subjected to forcing in both linear modes. Additionally, a method for assessing the accuracy of the prediction of the resonant crossing points is then introduced, and these predictions are then compared to responses found using numerical continuation.

1. Introduction

Predicting the dynamic responses of structures with nonlinear characteristics is a research field that has the ultimate aim of improving the design and efficiency of future structures. In this paper, the example of a two-degree-of-freedom coupled oscillator with cubic stiffness nonlinearities is considered. This system is representative of a range of applications in structural dynamics, see for example [1–3]. The system can exhibit internal resonances, associated vibration phenomena in structural elements such as beams, cables, membranes, plates and shells, as discussed, for example, in [4–7]. Although these phenomena are often undesirable, several studies consider whether they may be exploited to create nonlinear vibration absorbers, see [8–10] and references therein.

Approaches that are commonly used to study nonlinear structural dynamics include perturbation methods, nonlinear normal modes and normal form analysis [11–17]. However, these approaches are typically only applied to unforced, undamped systems as their application to forced, damped systems are, at best, algebraically intensive. As a result, including forcing and damping typically involves the use of numerical computation, and the advantages associated with analytical approaches are lost. In this work we present a technique for relating the unforced, undamped responses of coupled,

* Corresponding author.
E-mail address: tom.hill@bristol.ac.uk (T.L. Hill).

http://dx.doi.org/10.1016/j.jsv.2015.03.030
0022-460X/

nonlinear systems to the forced responses. This enables the approaches developed for free vibration responses to be adopted for forced cases, and provides a direct relationship between these free responses and the forced responses at resonance.

This paper follows the approach of [18], in which the unforced, undamped responses of the system are found analytically using the second-order normal form technique, first developed in [15]. These responses are referred to as *backbone curves* – for an early use of these see [19]. The stability of the backbone curves can be related to the stability of forced responses at resonance and may be described analytically. The second-order normal form technique requires that the nonlinear terms are small, relative to the linear terms. however, despite this restriction, the technique may still be used to model systems that exhibit complex nonlinear phenomena, such as bifurcations and internal resonance, see [18,20].

The relationship between the forced responses and the backbone curves is found using an analytical energy-based approach, which provides an approximate description of the forced responses at resonance – responses that are of particular interest in engineering. It also enables the prediction of nonlinear features such as isolas [21]. We note that several other studies have considered energy analysis of coupled nonlinear oscillators, typically in the context of vibration suppression. See, for example, [8–10] and references therein. The technique used here was first discussed in [22] where it is used as an analytical method for the design and optimisation of forced responses. Along with developing the technique, we also consider its inherent assumptions and introduce an analytical method for quantifying the errors associated with these.

The paper is structured as follows. In Section 2 we provide a brief description of how the second-order normal form technique is applied to forced systems. This is followed by a discussion of the dynamic response of a two degree-of-freedom oscillator with cubic nonlinearities. It is then shown how the features of the forced responses are related to the backbone curves of the system. Then in Section 3, the energy-based analysis is presented, leading to a method for approximating the forced response of the system at resonance. Finally conclusions are drawn in Section 4. For conciseness, the second-order normal form technique is not detailed in the main text, but summarised in Appendix A.

2. Backbone curves of an example system

In this paper we base our discussions around an example system, namely a forced and damped two-mass oscillator with a symmetric structure, as shown in Fig. 1. Two identical nonlinear springs, with force–deflection relationships $F=k(\Delta x)+\kappa(\Delta x)^3$, ground the masses, and one nonlinear spring, with force–deflection relationship $F=k_2(\Delta x)+\kappa_2(\Delta x)^3$, connects the masses. Two identical linear viscous dampers also ground the masses (damping constants c), and a third damper connects the two masses (damping constant c_2). The masses are both forced at frequency Ω, and at amplitudes P_1 and P_2 as shown in Fig. 1.

Whilst the system considered here is symmetric with cubic nonlinearities, the second-order normal form technique may also be applied to systems with asymmetries and other polynomial nonlinearities – provided the system has an underlying linear structure and the assumption of weak-nonlinearity is not violated [15]. Furthermore, the technique may be extended to include harmonic responses and may be computed to a higher-order of accuracy [23]; however, for the response range considered here, a good level of accuracy is achieved without these extensions.

2.1. Calculating the backbone curves

In this paper we use the second-order normal form technique to find the approximate dynamic behaviour of the example system. This technique consists of a series of transforms applied to the equations of motion, and results in approximate expressions for the resonant modal equation of motion describing the dynamics of the fundamental components of the linear modal coordinates of the system. These expressions can be solved to find the fundamental responses of the underlying linear modes which can then be used, along with the inverse of the aforementioned transforms, to find the harmonics, the responses to non-resonant forcing, and the responses in the physical coordinates.

The second-order normal form technique has previously been used in [18] to find the backbone curves of this system. In this section we provide a brief outline of the application of this technique to the forced and damped example system, whilst a more complete description is given in Appendix A. For a detailed description of the application of the second-order normal form technique to more general nonlinear systems, see [15,24].

We write the equation of motion for the example system in the form

$$\mathbf{M}\ddot{\mathbf{x}}+\mathbf{K}\mathbf{x}+\mathbf{N}_x(\mathbf{x},\dot{\mathbf{x}})=\mathbf{P}_x\cos(\Omega t), \tag{1}$$

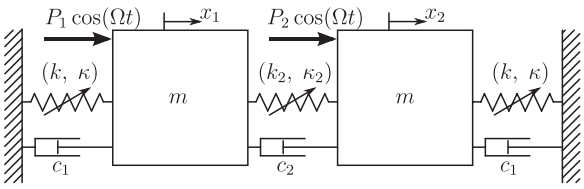

Fig. 1. A schematic diagram of a forced, nonlinear two-degree-of-freedom oscillator with a symmetric structure.

where $\mathbf{x}$ is a vector of physical displacements, $\mathbf{M}$ and $\mathbf{K}$ are the mass and stiffness matrices respectively, $\mathbf{N}_x$ is a vector of nonlinear and damping terms, $\mathbf{P}_x$ is a vector of forcing amplitudes and Ω is the forcing frequency.

The first step of the technique is to apply the linear modal transform $\mathbf{x}=\mathbf{\Phi q}$, where $\mathbf{\Phi}$ is a modeshape matrix and $\mathbf{q}$ is a vector of linear modal displacements. The ith column of $\mathbf{\Phi}$ is the modeshape of the ith linear mode, $\mathbf{p}_i$. Due to the symmetry of the system considered here the modeshapes may be written as $\mathbf{p}_1^T=[1,1]$ and $\mathbf{p}_2^T=[1,-1]$, such that the masses are in-phase and in anti-phase for responses in the first and second linear modes respectively. Note that here we use the term *mode* with reference to the underlying linear modes of the system. Applying this transform to Eq. (1) results in the modal equation of motion, written as

$$\ddot{\mathbf{q}}+\mathbf{\Lambda}q+\mathbf{N}_q(\mathbf{q},\dot{\mathbf{q}})=\mathbf{P}_q\cos(\Omega t), \tag{2}$$

where $\mathbf{\Lambda}$ is a diagonal matrix, whose ith leading diagonal element is the square of the ith linear natural frequency, ω_{ni}^2, $\mathbf{N}_q$ is a vector of nonlinear terms, and $\mathbf{P}_q$ is a vector of modal forcing amplitudes.

For the system considered here the next step, the forcing transform, is unity; therefore it is simply written as $\mathbf{q}=\mathbf{v}$. Applying this to Eq. (2) gives

$$\ddot{\mathbf{v}}+\mathbf{\Lambda}v+\mathbf{N}_v(\mathbf{v},\dot{\mathbf{v}})=\mathbf{P}_v\cos(\Omega t), \tag{3}$$

where $\mathbf{N}_v(\mathbf{v},\dot{\mathbf{v}})=\mathbf{N}_q(\mathbf{q},\dot{\mathbf{q}})$ and $\mathbf{P}_v=\mathbf{P}_q$.

The final step is the nonlinear near-identity transform $\mathbf{v}=\mathbf{u}+\mathbf{h}$ where $\mathbf{u}$ and $\mathbf{h}$ are the fundamental and harmonic components of $\mathbf{v}$ respectively. In the example considered here, the harmonics are sufficiently small that their influence on the fundamental component, and their contribution to the overall response, is negligible. Therefore, we can justifiably neglect the harmonics by writing $\mathbf{v}=\mathbf{u}$.

Assuming that the fundamental response of the ith linear mode is sinusoidal we may write

$$u_i=u_{ip}+u_{im}=\frac{U_i}{2}\left(\mathrm{e}^{+\mathrm{j}(\Omega t-\phi_i)}+\mathrm{e}^{-\mathrm{j}(\Omega t-\phi_i)}\right), \tag{4}$$

where U_i and ϕ_i are the fundamental response amplitude and phase of the ith mode respectively and we have assumed that the fundamental frequency of all modes is at the forcing frequency, Ω – i.e. the response frequency ratio is 1:1. This assumption is also motivated by the fact that the linear natural frequencies are close. For systems with well-separated modes, different response frequency ratios (i.e. n:m) will need to be selected [18].

The result of the nonlinear near-identity transform is the resonant equation of motion, written as

$$\ddot{\mathbf{u}}+\mathbf{\Lambda}\mathbf{u}+\mathbf{N}_u(\mathbf{u},\dot{\mathbf{u}})=\mathbf{P}_u\cos(\Omega t), \tag{5}$$

where $\mathbf{N}_u(\mathbf{u},\dot{\mathbf{u}})$ is a vector of resonant nonlinear terms and $\mathbf{P}_u=\mathbf{P}_q$. In Appendix A it is shown that $\mathbf{N}_u$ may be written as

$$\mathbf{N}_u=2\zeta\begin{pmatrix}\omega_{n1}\dot{u}_1\\ \omega_{n2}\dot{u}_2\end{pmatrix}+\frac{3\kappa}{m}\begin{pmatrix}u_{1p}u_{1m}u_1+2u_{2p}u_{2m}u_1+u_{1p}u_{2m}^2+u_{1m}u_{2p}^2\\ \gamma u_{2p}u_{2m}u_2+2u_{1p}u_{1m}u_2+u_{1p}^2u_{2m}+u_{1m}^2u_{2p}\end{pmatrix}, \tag{6}$$

where $\gamma=1+8\kappa_2/\kappa$ and ζ is the modal damping ratio, which is assumed to be equal for both modes.

Using the resonant equation of motion, Eq. (5), substituting in Eqs. (4) and (6) and setting the forcing and damping to zero, we can find the backbone curves. For this system we find four backbone curves; labelled $S1$, $S2$, $S3^+$ and $S3^-$. The *single-mode* backbone curves $S1$ and $S2$ are composed only of the first and second linear modal coordinates respectively and are calculated using

$$S1:\quad U_2=0,\quad \Omega^2=\omega_{n1}^2+\frac{3\kappa}{4m}U_1^2, \tag{7}$$

$$S2:\quad U_1=0,\quad \Omega^2=\omega_{n2}^2+\frac{3\kappa\gamma}{4m}U_2^2. \tag{8}$$

The *mixed-mode* backbone curves $S3^+$ and $S3^-$ (or $S3^\pm$ when referring to both) contain contributions from both linear modal coordinates. These have identical frequency–amplitude relationships, given by

$$S3^\pm:\quad U_1^2=\left(1-4\frac{\kappa_2}{\kappa}\right)U_2^2-\frac{2m}{3\kappa}(\omega_{n2}^2-\omega_{n1}^2), \tag{9a}$$

$$\Omega^2=\frac{3\omega_{n1}^2-\omega_{n2}^2}{2}+\frac{3(\kappa-\kappa_2)}{m}U_2^2, \tag{9b}$$

whilst the modal coordinates on $S3^+$ are in-phase, and on $S3^-$ the modes are in anti-phase, such that we may write

$$S3^+:\ |\phi_1-\phi_2|=0,\qquad S3^-:\ |\phi_1-\phi_2|=\pi. \tag{10}$$

The existence of more than one single-mode backbone curve is a feature of symmetric systems. For an example of the second-order normal form technique applied to an asymmetric structure, in which all backbone curves contain multiple modes, see [22].

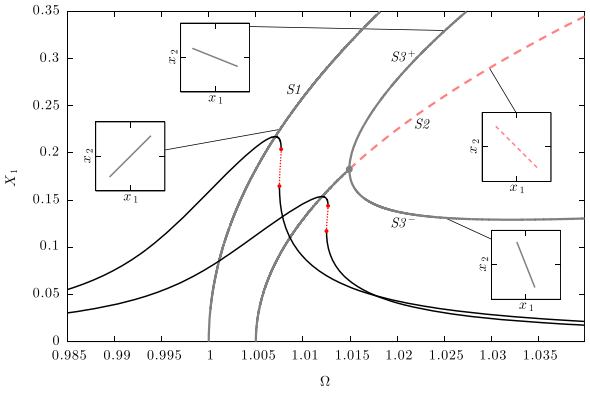

Fig. 2. Backbone curves and forced responses for the system where $m=1$, $\omega_{n1}=1$, $\omega_{n2}=1.005$, $\kappa=0.4$ and $\kappa_2=0.05$. The results are shown in the projection of the forcing and response frequency, Ω, against the amplitude of displacement of the first mass, X_1. Solid-grey and dashed-red lines represent stable and unstable backbone curves respectively and a grey bullet represents a symmetry-breaking bifurcation. Two forced responses, with modal damping $\zeta=0.004$ and forcing amplitudes $\mathbf{P}_q^T=[0.00175,0]$ and $\mathbf{P}_q^T=[0,0.00125]$, envelop the backbone curves $S1$ and $S2$ respectively. The stable and unstable forced responses are represented by solid-black and dotted-red lines respectively, and red bullets represent fold bifurcations. Four embedded plots, all in the projection x_1 against x_2, show responses of the system on the four backbone curves. (For interpretation of the references to colour in this figure caption, the reader is referred to the web version of this paper.)

Table 1
The forcing amplitudes and modal damping ratios for the two forced responses.

Single-mode forcing case	$P_q^T=[0,0.006]$	$\zeta=0.004$
Mixed-mode forcing case	$P_q^T=[0.0025,0.00375]$	$\zeta=0.004$

2.2. Structure of the backbone curves

We now use two simple forced responses, which have been calculated numerically, to demonstrate how they relate to the backbone curves, calculated using Eqs. (7)–(10). Fig. 2 shows the backbone curves of the two-degree-of-freedom system with the parameters $m=1$, $\omega_{n1}=1$, $\omega_{n2}=1.005$, $\kappa=0.4$ and $\kappa_2=0.05$, as used in [18], in the projection Ω against X_1.

As described in [18], a bifurcation, denoted by a grey bullet, connects $S2$ to $S3^{\pm}$. In this projection this is a symmetry-breaking bifurcation and leads to a loss of stability of $S2$, shown by a dashed-red line, and the emergence of the stable branches of $S3^{\pm}$, shown by solid-grey lines. To demonstrate the physical behaviour represented by each backbone curve, four embedded plots are shown in Fig. 2 in the projection x_1 against x_2, which represents the physical displacements of the two masses. It can be seen that, for $S1$ and $S2$, the responses shown in the embedded plots are in the first and second linear modeshapes respectively, i.e. the two physical coordinates respond at the same amplitude and are in-phase and in anti-phase respectively. The embedded plots demonstrating the responses on $S3^+$ and $S3^-$ both show a composition of the two modes, as the two masses respond at different amplitudes. The properties of the system that govern these backbone curves remain constant throughout this paper, hence these backbone curves remain constant for all the subsequent examples.

Fig. 2 also shows the forced response branches for the system under two different forcing cases: one in which $\mathbf{P}_q^T=[0.00175,0]$ and the other where $\mathbf{P}_q^T=[0,0.00125]$. In the first of these cases, only the first mode is forced, and in the latter case the forcing is directly in the second mode, hence we refer to these as *single-mode forcing* cases. In both instances the modal damping ratio is given by $\zeta=0.004$. It can be seen from Fig. 2 that these single-mode forcing cases lead to responses that envelop the single-mode backbone curves, such that the first-mode-only forced response branch envelops $S1$, and the second-mode-only branch envelops $S2$. The stable and unstable portions of the forced response branches are represented by solid-black and dotted-red lines respectively, and red bullets represent fold bifurcations.

We note that the forced solutions shown in Fig. 2, along with their stability and bifurcations, were calculated using the numerical continuation software AUTO-07p [25]. The high level of agreement between the forced responses (calculated numerically and including harmonics) and the backbone curves (calculated analytically and neglecting harmonics) indicates that, at such amplitudes, the assumptions made in the computation of the backbone curves are justifiable. For responses at higher amplitudes, it is likely that these assumptions would be weakened. The associated error could be reduced by including harmonics and/or computing the second-order normal form technique to a higher degree of accuracy [23].

As the forced responses shown in Fig. 2 consist of individual modes, referred to as *single-mode responses*, their behaviour is relatively simple and can be described using single-degree-of-freedom models. More complex phenomena are observed for *mixed-mode responses*, which can be seen for either mixed-mode forcing, or when single-mode forcing results in interactions with mixed-mode backbone curves, such as $S3^{\pm}$. These two cases are considered in the next section.

2.3. Mixed-mode responses of the forced system

We now consider two forcing cases that result in mixed-mode responses. The forcing amplitudes and modal damping ratios are given in Table 1 which defines the *single-mode forcing case*, in which only the second mode is directly forced, and the *mixed-mode forcing case*, in which both modes are forced. Note that the forcing amplitudes described in Table 1 are considerably larger than those used for the responses shown in Fig. 2. The response branches of these two forcing cases are shown in Figs. 3 and 4, along with the backbone curves of the system.

As in Fig. 2, the stable and unstable backbone curves in Figs. 3 and 4 are represented by solid-grey and dashed-red lines respectively, and the bifurcation from $S2$ onto $S3^{\pm}$ is indicated with a grey bullet. The stable and unstable forced responses are shown by thin-black lines and dotted-red lines respectively. The bifurcation points, from single-mode forced response branches onto mixed-mode branches, are represented by large-black bullets, whilst red bullets and blue asterisks are used to represent fold and torus bifurcations respectively. As in Fig. 2, the backbone curves have been calculated analytically, using Eqs. (7)–(10), and the forced responses have been calculated numerically, using AUTO-07p. The good agreement, in both cases, between the forced response branches and the backbone curves again suggests that the assumptions used for the backbone curves are justifiable at these amplitudes. Furthermore, from the numerical solutions it is found that the magnitudes of the harmonics are less than 1 per cent of the magnitudes of the corresponding fundamental responses, in the region depicted in Fig. 3.

As with the forced responses in Fig. 2, those in Figs. 3 and 4 are governed by the backbone curves. Additionally, in Fig. 3, a Duffing-like response branch, composed only of the second mode, envelops *S2*; however unlike in Fig. 2, this second-mode-only branch crosses *S2* above the bifurcation onto $S3^{\pm}$. Two bifurcation points on this single-mode forced response branch

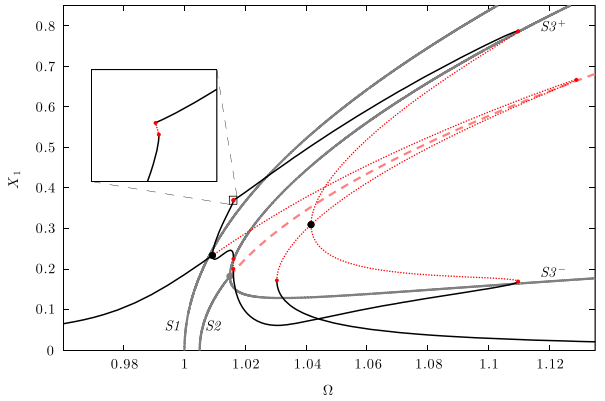

Fig. 3. Backbone curves and forced responses for the single-mode forcing case, shown in the projection of the forcing and response frequency, Ω, against the amplitude of displacement of the first mass, X_1. Solid-grey and dashed-red lines represent stable and unstable backbone curves respectively and a grey bullet shows the bifurcation on *S2*. Solid-black and dotted-red lines represent stable and unstable forced responses respectively. Red bullets represent fold bifurcations and large-black bullets show the bifurcations from the second-mode-only forced response onto the mixed-mode forced response. An embedded plot is used to detail the forced responses near two fold bifurcations. (For interpretation of the references to colour in this figure caption, the reader is referred to the web version of this paper.)

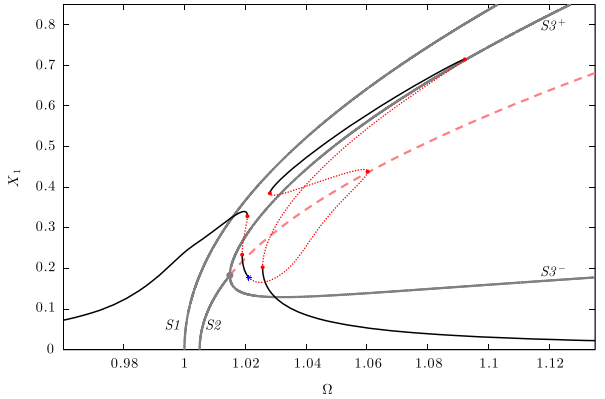

Fig. 4. Backbone curves and forced responses for the mixed-mode forcing case, shown in the projection of the forcing and response frequency, Ω, against the amplitude of displacement of the first mass, X_1. Solid-grey and dotted-red lines represent stable and unstable backbone curves respectively and a grey bullet shows the bifurcation on *S2*. Solid-black and dotted-red lines represent stable and unstable forced responses respectively. Blue asterisks and red bullets represent torus and fold bifurcations respectively. (For interpretation of the references to colour in this figure caption, the reader is referred to the web version of this paper.)

lead to mixed-mode, internally resonant, response branches that tend towards $S3^{\pm}$. These bifurcation points correspond to a loss of stability of the single-mode branch, which then crosses the unstable section of $S2$. For the forced responses in Fig. 4, in which both modes are forced, it can be seen that the response branches are governed by both $S1$ and $S2$. Due to the mixed-mode forcing, there are no separate, internally resonant, branches.

The mixed- and single-mode forcing cases demonstrate that the backbone curves of a system provide a simplified interpretation of the underlying dynamics of the forced responses. However, backbone curves alone cannot be used to quantify features of specific forced responses, such as calculating the amplitude at resonance under particular forcing conditions. The following section investigates a technique that may be used, in conjunction with backbone curve analysis, to quantify the behaviour of a forced system.

3. Energy transfer analysis

To understand the relationship between the forced responses at resonance and the backbone curves of a system, we assume that they share solutions at particular points, i.e. there exists one or more intersection points between the forced response branches and the backbone curves. We call these *resonant crossing points*. Therefore, in this context, the backbone curves represent loci of potential forced responses. Using this assumption, for each potential forced response we may calculate the energy-balance between the energy input (due to the external forcing) and the dissipated energy (due to the forcing and damping). We refer to this as the *net energy gain*, and it is representative of the energy transfer of the entire system, rather than the energy transfer between individual coordinates. For a steady-state response, the net energy gain over one period must be zero. Hence, any backbone curve response that satisfies this condition must also represent a valid forced solution, and so it must represent a resonant crossing point.

3.1. Calculating the energy transfer

We define a term that allows the exchange of energy into or out of the system as an *external transfer term* which, for the system considered here, is that describing the forcing and damping. The kth external transfer term in the modal equation of motion of the ith mode is written as $f_{E,ik}(t)$, hence the net energy gain due to this term over one period may be calculated as

$$E_{E,ik} = \int_0^T f_{E,ik}(t)\dot{q}_i(t)\,\mathrm{d}t, \tag{11}$$

where $\dot{q}_i(t)$ is the velocity of the ith linear mode and T is the period of the response. Here the harmonics are assumed to be negligible, allowing us to write $q_i = u_i = U_i\cos(\Omega t - \phi_i)$, see Eq. (4). Additionally, the external transfer terms (i.e. the forcing and damping terms in the modal equation of motion) for this system may all be written in the form

$$f_{E,ik} = F_{E,ik}\cos(\Omega t - \psi_{E,ik}), \tag{12}$$

where $F_{E,ik}$ and $\psi_{E,ik}$ are the amplitude and phase of $f_{E,ik}$ respectively. A number of other forms exist for external transfer terms, such as those for parametric forcing, however they are not considered here. The responses of the linear modal coordinates are at a frequency ratio of 1:1 in the example system. More generally, for a response at ratio n:m, the period, T, must be such that a complete number of cycles are captured for both modes.

Substituting Eq. (12) into Eq. (11), we write that the energy transfer out of the ith mode, due to the kth external transfer term, may be calculated as

$$E_{E,ik} = \frac{T}{2}F_{E,ik}U_i\Omega\sin(\phi_i - \psi_{E,ik}). \tag{13}$$

As the total net energy gain of the system must be zero, we may write

$$\sum_{i=1}^{I}\left\{U_i\sum_{k=1}^{K_{E,i}}\left\{F_{E,ik}\sin(\phi_i - \psi_{E,ik})\right\}\right\} = 0, \tag{14}$$

where $K_{E,i}$ is the number of external transfer terms in the ith modal equation of motion and I represents the total number of linear modes.

3.2. Energy transfer analysis applied to the example system

From Eqs. (5) and (6) it can be seen that the external transfer terms of the ith modal equation of motion may be written as

$$f_{E,i1} = 2\zeta\omega_{ni}\dot{u}_i, \quad f_{E,i2} = -P_{qi}\cos(\Omega t), \tag{15}$$

where P_{qi} is the ith element of $\mathbf{P}_q$. These may be expressed in the form of Eq. (12), giving

$$F_{E,i1} = -2\Omega\zeta\omega_{ni}U_i, \quad F_{E,i2} = -P_{qi}, \quad \psi_{i1} = \phi_i + \pi/2, \quad \psi_{i2} = 0. \tag{16}$$

Now, using Eq. (14) we may define the relationship

$$P_{q1}U_1\sin(\phi_1)+P_{q2}U_2\sin(\phi_2)=2\zeta\Omega\left(U_1^2\omega_{n1}+U_2^2\omega_{n2}\right). \tag{17}$$

To find the phases, ϕ_i, we consider the resonant equation of motion, Eq. (5), which may, for the ith mode, be written as

$$\sum_{k=1}^{K_{B,i}}\{f_{B,ik}\}+\sum_{k=1}^{K_{E,i}}\{f_{E,ik}\}=0, \tag{18}$$

where in the ith modal equation there are $K_{B,i}$ *internal transfer terms*, written as $f_{B,ik}$. In the system considered here, the internal transfer terms are those that do not describe forcing and damping, i.e. the terms that describe the backbone curves. As we are assuming that the forced responses and backbone curves share solutions at the resonant crossing points, it follows that

$$\sum_{k=1}^{K_{B,i}}\{f_{B,ik}\}=0 \quad \text{and} \quad \sum_{k=1}^{K_{E,i}}\{f_{E,ik}\}=0. \tag{19}$$

Note that the accuracy of this assumption will be discussed later in Section 3.3. Now, using Eq. (15), we may write

$$2\zeta\Omega\omega_{ni}U_i\sin(\Omega t-\phi_i)+P_{qi}\cos(\Omega t)=0, \tag{20}$$

which requires that $\phi_i=\pi/2$. Using this, Eq. (17) leads to

$$P_{q1}U_1+P_{q2}U_2=2\zeta\Omega\left(U_1^2\omega_{n1}+U_2^2\omega_{n2}\right). \tag{21}$$

To find a crossing point on $S1$, we substitute Eq. (7) into Eq. (21), which may be written as

$$\zeta^2\omega_{n1}^2\frac{3\kappa}{m}U_1^4+4\zeta^2\omega_{n1}^4U_1^2-P_{q1}^2=0, \tag{22}$$

and solved for U_1. Similarly, substituting Eq. (8) into Eq. (21) allows a resonant crossing point on $S2$ to be found using

$$\zeta^2\omega_{n2}^2\frac{3\kappa\gamma}{m}U_2^4+4\zeta^2\omega_{n2}^4U_2^2-P_{q2}^2=0. \tag{23}$$

Although not shown here, a similar approach can be taken to obtain an expression to find the resonant crossing points on $S3^{\pm}$, by substituting Eq. (9b) into Eq. (21).

For the single-mode forcing case, when $P_{q1}=0$, it can be seen from Eq. (22) that the crossing point on $S1$ occurs at $U_1=0$, i.e. responses on $S1$ consist only of the first mode, thus $S1$ does not meet any forced response that is not forced in the first mode. For the mixed-mode forcing case, in which the system is forced in both modes, it can be seen that both $S1$ and $S2$ will be crossed.

Figs. 5 and 6 show the resonant crossing point predictions for the single- and mixed-mode forcing cases respectively. Both figures use the projection of the forcing frequency, Ω, against the amplitude of displacement of the first mass, X_1. These figures can be compared directly with Figs. 3 and 4, as they share the same backbone curves and forced response curves. Figs. 5 and 6 show the predicted resonant crossing points, along with embedded plots in the projection of x_1 against x_2. These embedded plots compare the responses at the crossing points on the backbone curves with the forced responses near

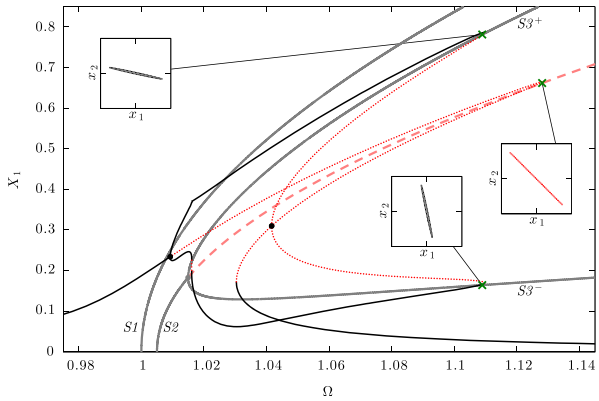

Fig. 5. Resonant crossing point predictions for the single-mode forcing case, shown in the projection of the forcing frequency, Ω, against the amplitude of displacement of the first mass, X_1. Solid-grey and dashed-red lines represent stable and unstable backbone curves respectively and a grey bullet represents the symmetry-breaking bifurcation. Solid-black and dotted-red lines show stable and unstable forced responses respectively. Green crosses show the predicted resonant crossing points. Three embedded plots, in the projection x_1 against x_2, show comparisons between the backbone curve responses at the crossing points, and the forced responses that are nearest the crossing points. (For interpretation of the references to colour in this figure caption, the reader is referred to the web version of this paper.)

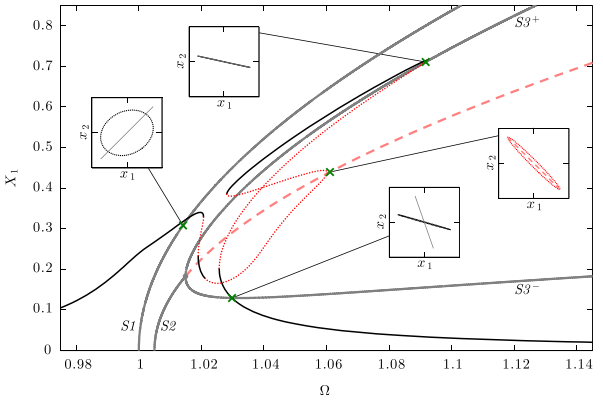

Fig. 6. Resonant crossing point predictions for the mixed-mode forcing case, shown in the projection of the forcing frequency, Ω, against the amplitude of displacement of the first mass, X_1. Solid-grey and dashed-red lines represent stable and unstable backbone curves respectively and a grey bullet represents the symmetry-breaking bifurcation. Solid-black and dotted-red lines show stable and unstable forced responses respectively. Green crosses show the predicted resonant crossing points. Four embedded plots, in the projection x_1 against x_2, show comparisons between the backbone curve responses at the crossing points, and the forced responses that are nearest the crossing points. (For interpretation of the references to colour in this figure caption, the reader is referred to the web version of this paper.)

the crossing points. Note that the forced responses shown in the embedded plots are those which are closest to the resonant crossing points in the projection Ω against X_1.

Figs. 5 and 6 demonstrate that the majority of resonant crossing points for these responses appear to be predicted with a good degree of accuracy; however, not all of the predictions shown are exact. Two sources of inaccuracy are the assumptions that the harmonics are negligible and that the nonlinear terms are small (made in second-order normal form technique). As previously discussed, the errors associated with these can be reduced by including harmonics and calculating the normal form technique to a higher degree of accuracy. In most instances there is also an error introduced by the assumption, made in the energy transfer analysis, that the forced responses and backbone curves share solutions at the resonant crossing points. In three embedded plots in Fig. 6 and, to a much lesser extent, in two embedded plots in Fig. 5, it is clear that the forced responses and backbone curves have distinct solutions. This demonstrates that the assumption made in the energy transfer analysis is not always accurate. The effect of this assumption is discussed in Section 3.3.

3.3. The limitation of energy transfer analysis

The energy transfer analysis presented here uses the assumption that the forced responses cross the backbone curves precisely, i.e. the forced responses and backbone curves share solutions at the resonant crossing points. The validity of this assumption can be examined, for the mixed-mode response cases, by considering the net energy transfer out of an individual mode, referred to as the *internal energy transfer*. As the backbone curves represent steady-state responses, the internal energy transfer, over one period, for any mode, must be zero. Hence, if a predicted resonant crossing point represents a response where, due to the forcing and damping, the internal energy transfer for any mode is non-zero then it cannot represent a forced response solution. Therefore, except in special cases, the predicted resonant crossing point is always an approximation to the true forced response.

We may estimate the accuracy of this approximation by calculating the change in phase that is necessary to accommodate this internal energy transfer. If the phase change is small then it suggests that the forced solution is in the near vicinity of the predicted crossing point, and hence we may assume that the approximation is justifiable. As the total net energy transfer out of any mode must be zero for any steady-state response, we may write

$$\sum_{k=1}^{K_{B,i}} \{E_{B,ik}\} + \sum_{k=1}^{K_{E,i}} \{E_{E,ik}\} = 0, \tag{24}$$

where $E_{B,ik}$ is the internal energy transfer out of mode i, due to the kth internal transfer term. Assuming $E_{B,ik}$ can be calculated in a similar manner to $E_{E,ik}$, i.e. using Eq. (13), then we may write

$$\sum_{k=1}^{K_{B,i}} F_{B,ik} \sin(\phi_i - \psi_{B,ik}) = -\sum_{k=1}^{K_{E,i}} F_{E,ik} \sin(\phi_i - \psi_{E,ik}), \tag{25}$$

where $F_{B,ik}$ and $\psi_{B,ik}$ are the amplitude and phase of the kth internal transfer term of the ith mode respectively. Considering the second mode of the system, Eq. (6) shows that the internal transfer terms are

$$f_{B,2,1} = \frac{3\kappa\gamma}{m} u_{2p} u_{2m} u_2, \quad f_{B,2,2} = \frac{6\kappa}{m} u_{1p} u_{1m} u_2,$$

$$f_{B,2,3} = \frac{3\kappa}{m}\left(u_{1p}^2 u_{2m} + u_{1m}^2 u_{2p}\right). \tag{26}$$

Expanding Eq. (26) using Eq. (4) it is found that

$$\begin{aligned} F_{B,2,1} &= \frac{3\kappa\gamma}{4m}U_2^3, \quad \psi_{B,2,1} = \phi_2, \\ F_{B,2,2} &= \frac{3\kappa}{2m}U_1^2 U_2, \quad \psi_{B,2,2} = \phi_2, \\ F_{B,2,3} &= \frac{3\kappa}{4m}U_1^2 U_2, \quad \psi_{B,2,3} = 2\phi_1 - \phi_2. \end{aligned} \tag{27}$$

Hence, substituting Eq. (16) (when $i=2$) and Eqs. (27) into Eq. (25) gives

$$\frac{3\kappa}{4m}U_1^2 U_2 \sin\left[2(\phi_2 - \phi_1)\right] = P_{q2}\sin(\phi_2) - 2\Omega\zeta\omega_{n2}U_2. \tag{28}$$

Using the assumption $\phi_2 = \pi/2$, from Eq. (20), we may write Eq. (28) as

$$\sin\left[2(\phi_1 - \phi_2)\right] = \frac{4m\left(2\Omega\zeta\omega_{n2}U_2 - P_{q2}\right)}{3\kappa U_1^2 U_2}. \tag{29}$$

This may then be used to calculate the phase difference that is required to allow the internal energy transfer for a predicted forced response.

For the single-mode forcing case (see Fig. 5) the predicted resonant crossing point on $S2$ is exact, as only the forced mode (i.e. the second mode) is responding and so there is no internal energy transfer.

The crossing points on $S3^{\pm}$ are both predicted at $\Omega = 1.1089$ (due to the symmetry of the system and the symmetric shape of the forcing) and both at amplitudes $[U_1, U_2] = [0.3084, 0.4729]$. Substituting this into Eq. (29) gives $\phi_1 - \phi_2 = 0.0663$ and $\phi_1 - \phi_2 = \pi + 0.0663$. As the phase differences on $S3^{\pm}$ are $\phi_1 - \phi_2 = 0, \pi$ we may determine that these predictions are good. This is reflected by the good agreement between the predicted and true (in this projection) crossing points in Fig. 5. The embedded plots in Fig. 5 also demonstrate the strong similarity between the solutions on the forced responses and the backbone curves, showing that the forced response branches are close to the backbone curves near the predicted resonant crossing points.

For the mixed-mode forcing case the crossing point on $S3^{+}$ is predicted at frequency $\Omega = 1.0917$ and at amplitudes $[U_1, U_2] = [0.2775, 0.4329]$, see Fig. 6. Substituting this into Eq. (29) gives $\phi_1 - \phi_2 = 0.0025$. As the modes on $S3^{+}$ are in-phase, this indicates that the crossing point prediction is extremely accurate, as indicated in Fig. 6. The reason for this high level of accuracy is that the shape of the forcing corresponds well with the shape of the response at this point on the backbone curve. Substituting the predicted crossing point on $S3^{-}$, given by frequency $\Omega = 1.0298$ and amplitudes $[U_1, U_2] = [0.1203, 0.2498]$, into Eq. (29) leads to $\sin\left[2(\phi_1 - \phi_2)\right] = -1.5503$, which has no solution in the real domain, indicating that the prediction of this point is highly inaccurate. Although Fig. 6 appears to show a good prediction of the $S3^{-}$ crossing point, this is simply a feature of the projection, Ω against X_1, i.e. the corresponding plot in X_2 would give a poor agreement. The inaccuracy of the crossing point on $S3^{-}$ is demonstrated by the embedded plot in Fig. 6, which shows that the forced and backbone curve solutions have little similarity. Furthermore, we expect the forced responses to approach the backbone curves when they reach resonance; however, the forced response crossing the $S3^{-}$ branch at this point is clearly not a resonant response, as confirmed by the analysis presented here.

4. Conclusions

In this paper, we consider how to interpret the forced responses of a nonlinear system using backbone curves – which capture the unforced, undamped responses – using an energy-based approach. To facilitate the discussion, a two-degree-of-freedom coupled oscillator with cubic stiffness nonlinearities has been considered.

The backbone curves were found using a normal form approach, which allows for the calculation of harmonics and higher orders of accuracy; however, for the example considered here, inclusion of these was not needed to achieve accurate results. Whilst the example system responds with a frequency ratio of 1:1, the techniques adopted here are not limited to such cases, and can more generally be applied to n:m resonant systems.

An energy-based analysis was then used to relate the forced responses to the backbone curves. This enables the identification of resonant crossing points where the two sets of responses could be equated. However, the assumption that the forced response branches and backbone curves intersect, which is key for this analysis, is not always true. This is demonstrated by showing that, although the branches appear to cross in certain projections, the solutions are not always shared.

In order to address this potential error, we proposed and demonstrated a phase difference calculation to estimate whether the forced solution is in the vicinity of the predicted resonant crossing point.

Beyond linking the forced response to the backbone curves, a further potential benefit of combining the energy and backbone curve analysis is that it may be used to find initial solutions from which to begin numerical continuation. This is especially beneficial for nonlinear phenomena such as isolas, which are difficult to find via conventional continuation

methods. Furthermore, as resonant forced responses are of particular interest in engineering, this approach provides a method for simplifying large, complex sets of forced response branches, into a set of individual, pertinent responses. This, along with the analytical nature of the methods presented here, may be used to simplify and accelerate the process of design and optimisation for nonlinear systems.

Acknowledgements

The authors would like to acknowledge the support of the EPSRC. T.L.H. is supported by an EPSRC DTA studentship. A.C. and D.J.W. are supported by EPSRC Grant EP/K003836/2 and S.A.N. is supported by EPSRC fellowship EP/K005375/1.

Appendix A. The method of second-order normal forms

In physical coordinates ($\mathbf{x}$) the equations of motion of this system may be written as

$$\mathbf{M}\ddot{\mathbf{x}}+\mathbf{K}\mathbf{x}+\mathbf{N}_x(\mathbf{x},\dot{\mathbf{x}})=\mathbf{P}_x\cos(\Omega t), \tag{A.1}$$

where $\mathbf{M}$ and $\mathbf{K}$ are the mass and stiffness matrices respectively, $\mathbf{P}_x$ is a vector of forcing amplitudes and $\mathbf{N}_x$ is a vector of nonlinear and damping terms, written as

$$\mathbf{N}_x=\begin{pmatrix}(c+c_2)\dot{x}_1-c_2\dot{x}_2\\(c+c_2)\dot{x}_2-c_2\dot{x}_1\end{pmatrix}+\begin{pmatrix}\kappa x_1^3+\kappa_2(x_1-x_2)^3\\\kappa x_2^3-\kappa_2(x_1-x_2)^3\end{pmatrix}. \tag{A.2}$$

The first step of the second-order normal form technique is to transform Eq. (A.1) from physical coordinates, $\mathbf{x}$, into linear modal coordinates, $\mathbf{q}$. This is achieved using the modeshape matrix $\mathbf{\Phi}$, whose ith column is the modeshape of the ith linear mode, to make the substitution $\mathbf{x}=\mathbf{\Phi}\mathbf{q}$ into Eq. (A.1) such that it may be written as

$$\ddot{\mathbf{q}}+\mathbf{\Lambda}q+\mathbf{N}_q(\mathbf{q},\dot{\mathbf{q}})=\mathbf{P}_q\cos(\Omega t), \tag{A.3}$$

where for the system considered here

$$\mathbf{\Phi}=\begin{bmatrix}1&1\\1&-1\end{bmatrix},\quad \mathbf{\Lambda}=\begin{bmatrix}\omega_{n1}^2&0\\0&\omega_{n2}^2\end{bmatrix},\quad \mathbf{P}_q=\begin{pmatrix}P_{q1}\\P_{q2}\end{pmatrix},$$
$$\mathbf{N}_q=\begin{pmatrix}2\zeta_1\omega_{n1}\dot{q}_1\\2\zeta_2\omega_{n2}\dot{q}_2\end{pmatrix}+\frac{\kappa}{m}\begin{pmatrix}q_1^3+3q_1q_2^2\\\gamma q_2^3+3q_1^2q_2\end{pmatrix}, \tag{A.4}$$

where ω_{ni}, P_{qi} and ζ_i are the linear natural frequency, linear modal forcing amplitude and linear modal damping constant of the ith linear mode respectively, and $\gamma=1+(8\kappa_2/\kappa)$. We may calculate P_{qi} and ζ_i using

$$\begin{pmatrix}P_{q1}\\P_{q2}\end{pmatrix}=\frac{1}{2m}\begin{pmatrix}P_1+P_2\\P_1-P_2\end{pmatrix},\quad \begin{pmatrix}2\zeta_1\omega_{n1}\\2\zeta_2\omega_{n2}\end{pmatrix}=\frac{1}{m}\begin{pmatrix}c\\c+2c_2\end{pmatrix}. \tag{A.5}$$

Here we assume that $\zeta_1=\zeta_2=\zeta$, i.e. $c_2=\zeta(\omega_{n2}-\omega_{n1})/m$.

The next step of the second-order normal form technique is the forcing transform ($\mathbf{q}\rightarrow\mathbf{v}$), which removes any non-resonant forcing terms from the equation of motion. For the parameters considered here the forcing is assumed to be in the vicinity of the linear natural frequencies, which are close – i.e. $\Omega\approx\omega_{n1}\approx\omega_{n2}$. Therefore all forcing terms are considered to be resonant, and the forcing transform is unity, i.e. $\mathbf{v}=\mathbf{q}$. For an example of the application of the forcing transform when forcing is away from resonance, see [15]. The resulting equation of motion is

$$\ddot{\mathbf{v}}+\mathbf{\Lambda}v+\mathbf{N}_v(\mathbf{v},\dot{\mathbf{v}})=\mathbf{P}_v\cos(\Omega t), \tag{A.6}$$

where $\mathbf{N}_v(\mathbf{v},\dot{\mathbf{v}})=\mathbf{N}_q(\mathbf{q},\dot{\mathbf{q}})$ and $\mathbf{P}_v=\mathbf{P}_q$.

The final step of the technique is the nonlinear near-identity transform ($\mathbf{v}\rightarrow\mathbf{u}$). This transform uses the substitution $\mathbf{v}=\mathbf{u}+\mathbf{h}$ where $\mathbf{u}$ and $\mathbf{h}$ describe the fundamental and harmonic components of $\mathbf{v}$ respectively. As we are assuming that the harmonics are negligible we may write $\mathbf{N}_v(\mathbf{v},\dot{\mathbf{v}})=\mathbf{N}_v(\mathbf{u},\dot{\mathbf{u}})$. Furthermore, we assume that the fundamental component of the ith mode is sinusoidal, such that it may be written as

$$u_i=u_{ip}+u_{im}=\frac{U_i}{2}\left(\mathrm{e}^{+\mathrm{j}(\Omega t-\phi_i)}+\mathrm{e}^{-\mathrm{j}(\Omega t-\phi_i)}\right), \tag{A.7}$$

where U_i and ϕ_i are the fundamental response amplitude and phase of the ith mode respectively. The subscripts p and m denote the positive (plus) and negative (minus) signs of the exponents respectively. Using Eqs. (A.4) and (A.7), we may substitute $q_i=u_{ip}+u_{im}$ into $\mathbf{N}_v(\mathbf{q},\dot{\mathbf{q}})$, giving

$$\mathbf{N}_v(\mathbf{u},\dot{\mathbf{u}})=\mathrm{j}2\zeta\Omega\begin{pmatrix}\omega_{n1}(u_{1p}-u_{1m})\\\omega_{n2}(u_{2p}-u_{2\,m})\end{pmatrix}+\frac{\kappa}{m}\begin{pmatrix}(u_{1p}+u_{1m})^3+3(u_{1p}+u_{1m})(u_{2p}+u_{2m})^2\\3(u_{1p}+u_{1m})^2(u_{2p}+u_{2m})+\gamma(u_{2p}+u_{2m})^3\end{pmatrix}. \tag{A.8}$$

The result of the nonlinear near-identity transform is the resonant equation of motion:

$$\ddot{\mathbf{u}} + \mathbf{\Lambda u} + \mathbf{N}_u(\mathbf{u}, \dot{\mathbf{u}}) = \mathbf{P}_u \cos(\Omega t), \tag{A.9}$$

in which all terms resonate at the forcing frequency, Ω, and $\mathbf{P}_u = \mathbf{P}_q$. To determine which nonlinear terms in Eq. (A.8) are resonant, and thus contribute to the vector $\mathbf{N}_u$, we first write $\mathbf{N}_v$ and $\mathbf{N}_u$ as

$$\mathbf{N}_v = \mathbf{n}_v \mathbf{u}^*, \quad \mathbf{N}_u = \mathbf{n}_u \mathbf{u}^*, \tag{A.10}$$

where $\mathbf{n}_v$ and $\mathbf{n}_u$ are matrices containing all the coefficients of the terms in $\mathbf{N}_v$ and $\mathbf{N}_u$ respectively, and $\mathbf{u}^*$ is a vector of all unique combinations of u_{ip} and u_{im}. The ℓth element of $\mathbf{u}^*$ may be written as

$$u^*_\ell = \prod_{k=1}^{2} \left\{ u_{kp}^{s_{\ell kp}} u_{km}^{s_{\ell km}} \right\}, \tag{A.11}$$

where $s_{\ell kp}$ and $s_{\ell km}$ are the exponents of u_{kp} and u_{km} in the ℓth element of $\mathbf{u}^*$ respectively. We may then calculate the matrix $\boldsymbol{\beta}$, used to find the resonant terms in $\mathbf{u}^*$, where element $\{i, \ell\}$ of $\boldsymbol{\beta}$ may be calculated as

$$\beta_{i\ell} = \left(\left[\sum_{k=1}^{2} \{ s_{\ell kp} - s_{\ell km} \} \right]^2 - 1 \right) \Omega^2. \tag{A.12}$$

If element $\{i, \ell\}$ of $\boldsymbol{\beta}$ is zero, then it corresponds to the coefficient of a resonant term, represented by element $\{i, \ell\}$ of $\mathbf{n}_v$. Therefore, we may populate $\mathbf{n}_u$ using

$$n_{u,i\ell} = \begin{cases} n_{v,i\ell} & \text{if } \beta_{i\ell} = 0, \\ 0 & \text{if } \beta_{i\ell} \neq 0. \end{cases} \tag{A.13}$$

Using Eqs. (A.8), (A.10), (A.11) and (A.12) we calculate $\mathbf{n}_v$, $\mathbf{u}^*$ and $\boldsymbol{\beta}$ as

$$\mathbf{n}_v^T = \frac{\kappa}{m} \begin{bmatrix} \alpha_1 & 0 \\ -\alpha_1 & 0 \\ 1 & 0 \\ 3 & 0 \\ 3 & 0 \\ 1 & 0 \\ 3 & 0 \\ 6 & 0 \\ 3 & 0 \\ 3 & 0 \\ 6 & 0 \\ 3 & 0 \\ 0 & \alpha_2 \\ 0 & -\alpha_2 \\ 0 & 3 \\ 0 & 3 \\ 0 & 6 \\ 0 & 6 \\ 0 & 3 \\ 0 & 3 \\ 0 & \gamma \\ 0 & 3\gamma \\ 0 & 3\gamma \\ 0 & \gamma \end{bmatrix}, \quad \mathbf{u}^* = \begin{bmatrix} u_{1p} \\ u_{1m} \\ u_{1p}^3 \\ u_{1p}^2 u_{1m} \\ u_{1p} u_{1m}^2 \\ u_{1m}^3 \\ u_{1p} u_{2p}^2 \\ u_{1p} u_{2p} u_{2m} \\ u_{1p} u_{2m}^2 \\ u_{1m} u_{2p}^2 \\ u_{1m} u_{2p} u_{2m} \\ u_{1m} u_{2m}^2 \\ u_{2p} \\ u_{2m} \\ u_{1p}^2 u_{2p} \\ u_{1p}^2 u_{2m} \\ u_{1p} u_{1m} u_{2p} \\ u_{1p} u_{1m} u_{2m} \\ u_{1m}^2 u_{2p} \\ u_{1m}^2 u_{2m} \\ u_{2p}^3 \\ u_{2p}^2 u_{2m} \\ u_{2p} u_{2m}^2 \\ u_{2m}^3 \end{bmatrix}, \quad \boldsymbol{\beta}^T = \Omega^2 \begin{bmatrix} 0 & - \\ 0 & - \\ 8 & - \\ 0 & - \\ 0 & - \\ 8 & - \\ 8 & - \\ 0 & - \\ 0 & - \\ 0 & - \\ 0 & - \\ 8 & - \\ - & 0 \\ - & 0 \\ - & 8 \\ - & 0 \\ - & 0 \\ - & 0 \\ - & 0 \\ - & 8 \\ - & 8 \\ - & 0 \\ - & 0 \\ - & 8 \end{bmatrix}, \tag{A.14}$$

where $\alpha_1 = \mathrm{j}2\zeta\Omega\omega_{n1}(m/\kappa)$ and $\alpha_2 = \mathrm{j}2\zeta\Omega\omega_{n2}(m/\kappa)$. An element in $\boldsymbol{\beta}$ containing a dash (–) corresponds to an element in $\mathbf{n}_v$ containing a zero – hence the value of the element in $\boldsymbol{\beta}$ is of no importance.

We can now identify all resonant terms as those corresponding to zero in $\boldsymbol{\beta}$ and use Eq. (A.13) to populate the matrix $\mathbf{n}_u$. Once we have found $\mathbf{n}_u$, we use Eqs. (A.10) and (A.14), calculate $\mathbf{N}_u$ as

$$\mathbf{N}_u = 2\zeta \begin{pmatrix} \omega_{n1} \dot{u}_1 \\ \omega_{n2} \dot{u}_2 \end{pmatrix} + \frac{3\kappa}{m} \begin{pmatrix} u_{1p} u_{1m} u_1 + 2u_{2p} u_{2m} u_1 + u_{1p} u_{2m}^2 + u_{1m} u_{2p}^2 \\ \gamma u_{2p} u_{2m} u_2 + 2u_{1p} u_{1m} u_2 + u_{1p}^2 u_{2m} + u_{1m}^2 u_{2p} \end{pmatrix}. \tag{A.15}$$

The backbone curves, i.e. the free responses of the system, may now be found by setting the forcing and damping to zero. Therefore, substituting Eq. (A.15) into the resonant equation of motion, Eq. (A.9), when $\zeta = 0$ and $\mathbf{P}_u^T = [0, 0]$, gives

$$\left[\omega_{n1}^2 - \Omega^2\right] u_1 + \frac{3\kappa}{m}\left(u_{1p}u_{1m}u_1 + 2u_{2p}u_{2m}u_1 + u_{1p}u_{2m}^2 + u_{1m}u_{2p}^2 \right) = 0, \tag{A.16a}$$

$$\left[\omega_{n2}^2 - \Omega^2\right] u_2 + \frac{3\kappa}{m}\left(\gamma u_{2p}u_{2m}u_2 + 2u_{1p}u_{1m}u_2 + u_{1p}^2 u_{2m} + u_{1m}^2 u_{2p}\right) = 0. \tag{A.16b}$$

Using Eq. (A.7), it is found that Eq. (A.16b) may each be written as

$$\Upsilon_i^+ \mathrm{e}^{+\mathrm{j}\Omega t} + \Upsilon_i^- \mathrm{e}^{-\mathrm{j}\Omega t} = 0, \tag{A.17}$$

where Υ_i^+ and Υ_i^- are complex conjugates. From Eq. (A.17) it can be seen that $\Upsilon_i^+ = 0$. Hence, using Eq. (A.16b) we may write

$$\left[\omega_{n1}^2 - \Omega^2 + \frac{3\kappa}{4m}\left\{ U_1^2 + U_2^2\left(2 + \mathrm{e}^{+\mathrm{j}2(\phi_1 - \phi_2)}\right)\right\}\right]\frac{U_1}{2}\mathrm{e}^{-\mathrm{j}\phi_1} = 0, \tag{A.18a}$$

$$\left[\omega_{n2}^2 - \Omega^2 + \frac{3\kappa}{4m}\left\{\gamma U_2^2 + U_1^2\left(2 + \mathrm{e}^{-\mathrm{j}2(\phi_1 - \phi_2)}\right)\right\}\right]\frac{U_2}{2}\mathrm{e}^{-\mathrm{j}\phi_2} = 0. \tag{A.18b}$$

Taking the imaginary parts of Eq. (A.18b) gives $\sin(2|\phi_1 - \phi_2|) = 0$. Therefore

$$\mathrm{e}^{\mathrm{j}2|\phi_1 - \phi_2|} = \cos(2|\phi_1 - \phi_2|) = \pm 1 = p, \tag{A.19}$$

where $p = +1$ corresponds to $|\phi_1 - \phi_2| = n\pi$ and $p = -1$ corresponds to $|\phi_1 - \phi_2| = (2n-1)\pi/2$, for $n \in \mathbb{Z}$. The case where $p = -1$ is investigated in [20] where it is shown that it does not yield a solution for the parameter values considered here. Hence, when $p = +1$, Eq. (A.18b) may be written as

$$\left[\omega_{n1}^2 - \Omega^2 + \frac{3\kappa}{4m}\left\{ U_1^2 + 3U_2^2\right\}\right] U_1 = 0, \tag{A.20a}$$

$$\left[\omega_{n2}^2 - \Omega^2 + \frac{3\kappa}{4m}\left\{\gamma U_2^2 + 3U_1^2\right\}\right] U_2 = 0. \tag{A.20b}$$

Two straightforward solutions exist when either $U_2 = 0$ or $U_1 = 0$, leading to two backbone curves denoted $S1$ and $S2$, characterised by

$$S1: \quad U_2 = 0, \quad \Omega^2 = \omega_{n1}^2 + \frac{3\kappa}{4m}U_1^2, \tag{A.21}$$

$$S2: \quad U_1 = 0, \quad \Omega^2 = \omega_{n2}^2 + \frac{3\kappa\gamma}{4m}U_2^2. \tag{A.22}$$

When both $U_1 \neq 0$ and $U_2 \neq 0$, Eq. (A.20b) may be written as

$$\Omega^2 = \omega_{n1}^2 + \frac{3\kappa}{4m}\left\{U_1^2 + 3U_2^2\right\} = \omega_{n2}^2 + \frac{3\kappa}{4m}\left\{\gamma U_2^2 + 3U_1^2\right\}. \tag{A.23}$$

This may be used to find two additional backbone curves – one in which the modes are in-phase and the other in which the modes are in anti-phase. These are denoted $S3^+$ and $S3^-$ (or $S3^\pm$ when referring to both). From Eq. (A.23), these have the frequency–amplitude relationship:

$$S3^\pm: \quad U_1^2 = \left(1 - 4\frac{\kappa_2}{\kappa}\right)U_2^2 - \frac{2m}{3\kappa}(\omega_{n2}^2 - \omega_{n1}^2), \tag{A.24a}$$

$$\Omega^2 = \frac{3\omega_{n1}^2 - \omega_{n2}^2}{2} + \frac{3(\kappa - \kappa_2)}{m}U_2^2, \tag{A.24b}$$

and the phase differences

$$S3^+: \ |\phi_1 - \phi_2| = 0, \quad S3^-: \ |\phi_1 - \phi_2| = \pi. \tag{A.25}$$

References

[1] M. Cartmell, *Introduction to Linear, Parametric and Nonlinear Vibrations*, Chapman and Hall, Berlin, Germany, 1990.
[2] J.J. Thomsen, *Vibrations and Stability: Advanced Theory, Analysis and Tools*, Springer, Berlin, Germany, 2003.
[3] D.J. Wagg, S.A. Neild, *Nonlinear Vibration with Control*, Springer-Verlag, Berlin, Germany, 2009.
[4] M. Amabili, *Nonlinear Vibrations and Stability of Shells and Plates*, Cambridge, 2008.
[5] R. Lewandowski, On beams, membranes and plates backbone curves in a cases of internal resonance, *Meccanica* 31 (3) (1996) 323–346, http://dx.doi.org/10.1007/BF00426994.

[6] N. Srinil, G. Rega, Nonlinear longitudinal/transversal modal interactions in highly extensible suspended cables, *Journal of Sound and Vibration* 310 (1–2) (2008) 230–242, http://dx.doi.org/10.1016/j.jsv.2007.07.056.
[7] C. Touzé, O. Thomas, A. Chaigne, Asymmetric non-linear forced vibrations of free-edge circular plates. Part 1: theory, *Journal of Sound and Vibration* 258 (4) (2002) 649–676, http://dx.doi.org/10.1006/jsvi.2002.5143.
[8] O. Gendelman, L.I. Manevitch, A.F. Vakakis, L. Bergman, A degenerate bifurcation structure in the dynamics of coupled oscillators with essential stiffness nonlinearities, *Nonlinear Dynamics* 33 (2003) 1–10, http://dx.doi.org/10.1023/A:1025515112708.
[9] G. Kerschen, J.J. Kowtko, D.M. McFarland, L.A. Bergman, A.F. Vakakis, Theoretical and experimental study of multimodal targeted energy transfer in a system of coupled oscillators, *Nonlinear Dynamics* 47 (1-3) (2007) 285–309, http://dx.doi.org/10.1007/s11071-006-9073-5.
[10] A.F. Vakakis, Inducing passive nonlinear energy sinks in vibrating systems, *Journal of Vibration and Acoustics* 123 (3) (2001) 324–332, http://dx.doi.org/10.1115/1.1368883.
[11] V.I. Arnold, *Geometrical Methods in the Theory of Ordinary Differential Equations*, Springer, New York, 1988.
[12] L. Jezequel, C.H. Lamarque, Analysis of nonlinear dynamic systems by the normal form theory, *Journal of Sound and Vibration* 149 (3) (1991) 429–459, http://dx.doi.org/10.1016/0022-460X(91)90446-Q.
[13] G. Kerschen, M. Peeters, J.C. Golinval, A.F. Vakakis, Nonlinear normal modes, Part I: a useful framework for the structural dynamicist, *Mechanical Systems and Signal Processing* 23 (1) (2009) 170–194, http://dx.doi.org/10.1016/j.ymssp.2008.04.002.
[14] A.H. Nayfeh, D.T. Mook, *Nonlinear Oscillations*, Wiley, New York, 1995.
[15] S.A. Neild, D.J. Wagg, Applying the method of normal forms to second-order nonlinear vibration problems, *Proceedings of the Royal Society A: Mathematical, Physical and Engineering Science* 467 (28) (2011) 1141–1163, http://dx.doi.org/10.1098/rspa.2010.0270.
[16] C. Pierre, D.Y. Jiang, S. Shaw, Nonlinear normal modes and their application in structural dynamics, *Mathematical Problems in Engineering* (2006) Article ID 10847, 15 pp. http://dx.doi.org/10.1155/MPE/2006/10847.
[17] C. Touzé, M. Amabili, Nonlinear normal modes for damped geometrically nonlinear systems: *application to reduced-order modelling of harmonically forced structures*, *Journal of Sound and Vibration* 298 (4-5) (2006) 958–981, http://dx.doi.org/10.1016/j.jsv.2006.06.032.
[18] A. Cammarano, T.L. Hill, S.A. Neild, D.J. Wagg, Bifurcations of backbone curves for systems of coupled nonlinear two mass oscillator, *Nonlinear Dynamics* 77 (1–2) (2014) 311–320, http://dx.doi.org/10.1007/s11071-014-1295-3.
[19] W.-Y. Tseng, J. Dugundji, Nonlinear vibrations of a buckled beam under harmonic excitation, *Journal of Applied Mechanics* 38 (2) (1971) 467–476, http://dx.doi.org/10.1115/1.3408799.
[20] T.L. Hill, A. Cammarano, S.A. Neild, D.J. Wagg, Out-of-unison resonance in weakly-nonlinear oscillators, *Proceedings of the Royal Society A: Mathematical, Physical and Engineering Sciences* 471 (2015) 20140659, http://dx.doi.org/10.1098/rspa.2014.0659.
[21] N.A. Alexander, F. Schilder, Exploring the performance of a nonlinear tuned mass damper, *Journal of Sound and Vibration* 319 (12) (2009) 445–462, http://dx.doi.org/10.1016/j.jsv.2008.05.018.
[22] T.L. Hill, A. Cammarano, S.A. Neild, D.J. Wagg, An analytical method for the optimisation of weakly nonlinear systems, *Proceedings of EURODYN 2014*, Porto, July 2014, pp. 1981–1988.
[23] S.A. Neild, D.J. Wagg, A generalized frequency detuning method for multidegree-of-freedom oscillators with nonlinear stiffness, *Nonlinear Dynamics* 73 (2013) 649–663, http://dx.doi.org/10.1007/s11071-013-0818-7.
[24] S.A. Neild, Approximate methods for analysing nonlinear structures, in: D.J. Wagg, L. Virgin (Eds.), *Exploiting Nonlinear Behavior in Structural Dynamics*, Springer, Vienna2012, pp. 53–109.
[25] E.J. Doedel, A.R. Champneys, T.F. Fairgrieve, Y.A. Kuznetsov, F. Dercole, B.E. Oldeman, R.C. Paffenroth, B. Sandstede, X.J. Wang, C. Zhang, AUTO-07P: Continuation and Bifurcation Software for Ordinary Differential Equations, Montreal, Concordia University, Canada, 2008. See ⟨http://cmvl.cs.concordia.ca⟩.